JOURNAL OF PROPULSION AND POWER
Vol. 27, No. 1, January–February 2011

Propulsive Performance of a Continuously Rotating Detonation Engine

Tae-Hyeong Yi,* Jing Lou,† and Cary Turangan†
Institute of High Performance Computing, Singapore 138632, Republic of Singapore
Jeong-Yeol Choi‡
Pusan National University, Busan 609-735, Republic of Korea
and
Piotr Wolanski§
Warsaw University of Technology, 00-665 Warsaw, Poland.

DOI: 10.2514/1.46686

Detonation waves propagating in an annular chamber are numerically studied to investigate the propulsive performance of a continuously rotating detonation-based propulsion system. Engine operating conditions are assumed for the inflow conditions of an air-breathing engine combustor. The influence of various design parameters on the propulsive performance is estimated where parametric variables include total pressure, total temperature, injection area ratio, axial chamber length and the number of detonation waves. An overall flowfield in the combustion chamber is analyzed to understand the dynamics of detonation propagation and the basic engine operation. The propulsive performance of a continuously rotating detonation engine is compared with that of a single-tube pulse detonation engine. It is shown that the thrust of the rotating detonation engine converges to an approximately constant value after stabilized. The propulsive performance of the engine is strongly dependent on the injection conditions, but it is weakly dependent on the axial chamber length and the number of detonation waves. It is found that the total impulse produced by the rotating detonation engine is higher than the pulse detonation engine at given conditions.

I. Introduction

DETONATION is a shock-induced combustion process in which some or all of the energy necessary to support the shock comes from the heat release of the combustion. The shock compresses the mixture and increases its temperature beyond the ignition point, which subsequently initiates the detonation and provides it with energy to be self-sustained. In terms of propulsion applications, a detonation-based engine has higher propulsive efficiency, wider operating ranges from low subsonic to high supersonic speed, and simpler and more compact combustor designs [1]. The most common type of a detonation-based propulsion system is pulse detonation engine (PDE). The principle of PDE is based on the detonation wave propagating in a tube where a near constant-volume heat addition produces a very high pressure and hence provides thrust [1]. Numerous PDE test beds and its variant concepts have been developed such as the rotary-valved single or multitube PDE [2,3], the pulsed detonation combustor-turbine hybrid system [4] and the multimode detonation-based propulsion system [5]. Although aspects such as the initiation of detonation, the geometry of a combustion system and the dynamics of detonation phenomena still constrain the development of PDE, a recent flight test of the Long E-Z aircraft powered by a four-tube PDE demonstrates its potential as one of future propulsion systems [6].

In addition to PDE, there have been alternative attempts to use detonation combustion into a propulsion system, called continuously rotating detonation engine (RDE). In some literatures [7,8], it is also called continuous spin detonation, but to avoid confusion with a classical spinning detonation that has helical motion in its front [9], the authors have used the term *continuously rotating detonation* in this study. RDE uses detonation waves that are continuously generated and propagated into the azimuthal direction of an annular chamber as long as a fuel-oxidizer mixture is supplied. It is operated at very high frequency, typically several kHz depending on chamber geometry, fuel-oxidizer type and injection conditions. RDE produces a roughly constant thrust and requires only a single initiation of detonation.

RDE has indeed been proposed as a substitute for liquid-propellant rocket or ramjet engine [8,10]. Factors such as fuel-oxidizer mixtures, combustion chamber geometry and mass flow rate determine the number of detonation fronts rotating inside the chamber and the dynamics of the detonation propagation [11]. A variety of aspects associated with the basic phenomenon of the rotating detonation have been experimentally and theoretically investigated by Bykovskii et al. [8,12], followed by the pioneering works of Voitsekhovskii [7] and Nicholls et al. [13]. The works of Bykovskii et al. were focused on the rotating detonation of various fuel mixtures such as hydrogen, propane, acetone and kerosene in rocket- and ramjet-type combustors. They found that the existence of continuously rotating detonation in the various mixtures depends on parameters such as the pressure in the chamber, the extended part of the chamber and the ambient pressure. Works on other important aspects include fuel injection method, the effects of different fuel-oxidizer mixtures, the initiation of detonation and the limits to which detonation is continuous. Wolanski et al. [14] and Wolanski [15] have also conducted experiments with various mixtures, mixture compositions and initial pressures in the chamber. They achieved the rotating detonation of an acetylene and oxygen mixture in a coaxial combustion chamber where the detonation velocity was close to its Chapman–Jouguet value. In terms of performance, Daniau et al. [10] experimented using GH_2-LO_2 and LHC-GO_2 mixtures and showed the thrust of 2750 N in a 50 mm diameter and 100 mm long chamber. Falempin and Daniau [11] also studied the use of liquid hydrogen and oxygen mixture in the

Received 10 August 2009; revision received 28 September 2010; accepted for publication 28 September 2010.

*Currently, Senior Research Engineer, Department of Advanced Aerodynamics and Structure, Korea Aerospace Research Institute, Daejeon 303-333, Republic of Korea. Senior Member AIAA.
†Senior Research Engineer, Fluid Dynamics, Large-Scale Complex Systems.
‡Professor, Department of Aerospace Engineering. Senior Member AIAA.
§Professor, Institute of Heat Engineering. Member AIAA.

performance as well as the use of composite materials to sustain the high temperature resulting from the detonation.

Owing to the complexity and difficulties to capture the phenomena of detonation continuously rotating in an annular chamber, only limited numerical efforts have been reported in literature. Amongst others are Zhdan et al. [16], who performed two-dimensional unsteady modeling of rotating detonation in an annular chamber with a hydrogen-oxygen mixture, and Davidenko et al. [17], who simulated rotating detonation in a 0.1×0.1 m chamber with the detailed kinetic model of a hydrogen and oxygen mixture using six species and seven reversible reactions. Davidenko used high-order weighted essentially nonoscillatory scheme coupled with a semi-implicit Runge–Kutta time integration method. He reported the effects of the injection parameters and chamber geometry on the detonation propagation and wall pressure. Recently, Hishida et al. [18] also numerically studied the detailed flowfield structure of rotating detonation in a 0.2×0.2 m chamber with the two-step chemistry of an argon-diluted hydrogen and oxygen mixture.

A computational model considered in the present work is based on Euler equations with source terms associated with chemical reactions. A chemical kinetic model is employed with a one-step, irreversible Arrhenius kinetics of a hydrogen-air mixture. To overcome stiffness due to chemical reactions, a time-operator splitting method is used. The rotating detonation engine is modeled in a two-dimensional chamber, which represents the outer area of an annular chamber used in the experiments [14]. As the objective of this work, the propulsive performance of the air-breathing type RDE is studied with a variety of design parameters to obtain the insight of behaviors and trends in RDE operations. Detailed flowfield structure including the properties of injected mixture and detonation wave in the chamber is described using baseline injection conditions, i.e., a total pressure of 10 atm, a total temperature of 500 K and an injection area ratio of 0.2. The thrust and specific impulse of the RDE are evaluated in terms of various injection conditions, axial chamber lengths and the number of detonation waves. For the parametric study of engine performance with injection conditions, a wide range of conditions is used as the total pressure of 5–15 atm, the total temperature of 300–500 K and the injection area ratio of 0.1–0.4. In the following section, the thrust and total impulse of the RDE with baseline conditions are compared with those generated by single-tube pulse detonation engine.

II. Mathematical Formulations and Physical Configurations

A. Governing Equations and Numerical Methods

Because only gasdynamic properties are considered in a combustion chamber, a one-step, irreversible Arrhenius kinetics is adopted for this study so that the ratio of specific heats and the equation of state obey the law of a calorically perfect gas. Moreover, the effect of transport properties such as the viscosity, thermal conduction and mass diffusion are ignored. Thus, the governing equations are two-dimensional, unsteady Euler equations with source terms due to chemical reactions. These equations are expressed in a vector form in Cartesian coordinates as

$$\frac{\partial \mathbf{Q}}{\partial t} + \frac{\partial \mathbf{F}}{\partial x} + \frac{\partial \mathbf{G}}{\partial y} = \mathbf{S} \tag{1}$$

where the conservative variable vector $\mathbf{Q}$, the convective flux vectors $\mathbf{F}$ and $\mathbf{G}$, and the source vector $\mathbf{S}$ are, respectively, given by

$$\mathbf{Q} = \begin{bmatrix} \rho \\ \rho u \\ \rho v \\ \rho E \\ \rho Y \end{bmatrix}, \quad \mathbf{F} = \begin{bmatrix} \rho u \\ \rho u^2 + p \\ \rho uv \\ \rho uH \\ \rho uY \end{bmatrix}, \quad \mathbf{G} = \begin{bmatrix} \rho v \\ \rho uv \\ \rho v^2 + p \\ \rho vH \\ \rho vY \end{bmatrix} \quad \text{and} \quad \mathbf{S} = \begin{bmatrix} 0 \\ 0 \\ 0 \\ 0 \\ \dot{\omega} \end{bmatrix} \tag{2}$$

In Eq. (2), ρ is the density, p is the pressure, u and v are the velocity components, and Y is the mass fraction of reactant. The mass fraction of the product is $1 - Y$. The total enthalpy H is defined as

$$H = E + \frac{p}{\rho} \tag{3}$$

where the total energy E is the sum of the internal energy and the kinetic energy, that is

$$E = \frac{p}{(\gamma - 1)\rho} + qY + \frac{1}{2}(u^2 + v^2) \tag{4}$$

In the above equation, γ is the ratio of specific heats and q is the total chemical energy release. The mass production rate $\dot{\omega}$ given in Eq. (2) is defined in the first-order Arrhenius form by

$$\dot{\omega} = \frac{\mathrm{d}Y}{\mathrm{d}t} = -K\rho Y \exp\left(\frac{-E_a}{RT}\right) \tag{5}$$

where K is the preexponential factor, E_a is the activation energy, R is the specific gas constant, and T is the temperature. Because the calorically perfect gas is assumed, the five thermodynamic and chemical parameters γ, q, R, K, and E_a given in Eqs. (4) and (5) are constant and their values are given in the following section.

In simulating detonation waves, numerical difficulty is usually encountered due to a wide range of temporal scale, which leads to numerical stiffness. To take care of stiffness, a time-operator splitting method is used. This method is widely adopted in detonation simulations since it is a robust method, works well with time-dependent problems, and allows existing codes to be directly applied to each step without any modification for source terms. However, the wrong propagating speed of discontinuities may be predicted if the accuracy of spatial and temporal terms is not sufficient [19,20]. For this case, one could use finer grid resolution to capture the proper propagation speed, or one could apply under-resolved schemes as proposed by Helzle et al. [19], Tosatto and Vigevano [20] and Berkenbosch et al. [21]. For the homogeneous partial differential equations given in the left side of Eq. (1), spatial and temporal terms are discretized using a finite volume method with a cell-centered scheme and a second-order, three-step Runge–Kutta method, respectively. The convective fluxes $\mathbf{F}$ and $\mathbf{G}$ at cell faces are integrated with the second-order MUSCL-based Roe scheme. The ordinary differential equation due to chemical reaction given in Eq. (5) can be solved exactly using separation of variables [22].

B. RDE Modeling and Injection Boundary Conditions

A combustion chamber modeled in this study is adopted from Davidenko et al. [17] and illustrated in Fig. 1a. It is assumed that a fresh fuel-oxidizer mixture is normally supplied through a large number of small injectors evenly mounted on the left closed-end of the chamber and combustion products are exhausted to the right open-end. The detonation tangentially transferred from an initiator propagates in the azimuthal direction of a chamber channel. For this study, a detonation is modeled in a two-dimensional chamber simplified by assuming that the distance between an inner and outer wall is infinitely small. The two-dimensional chamber is shown in Fig. 1b where the chamber length in the azimuthal direction is the same as the circumference of the actual annular chamber used in the experiments [14]. Periodic boundary conditions are, thus, applied on the upper and lower boundaries of a computational domain. The slip boundary conditions are imposed at the left closed-end, while either subsonic or supersonic outflow boundary conditions are applied to the right open-end, depending on the local Mach number at the exit.

In the operation of the RDE, a fuel-oxidizer mixture is continuously supplied from the injectors to the chamber. As a result, it is formed as the triangle layer of the fresh mixture and flows in the axial direction. The successive detonation waves burn the injected mixture and propagates in the azimuthal direction. If the mixture layer is too small or too large, which depends on the mass flow rate of a mixture, the operation of the RDE will fail. To keep supplying the proper

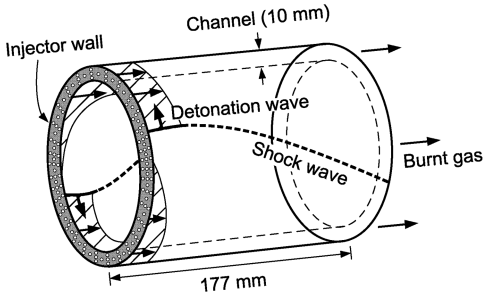

a) RDE chamber modeled in the study

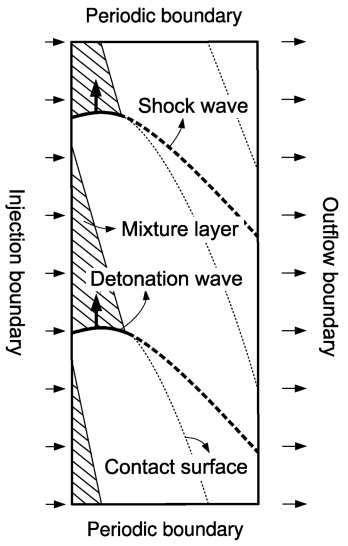

b) Computational setup in a two-dimensional, simplified RDE chamber

Fig. 1 Schematic of a RDE chamber and its physical and numerical configurations: the chamber has an inner and outer diameter of 130 and 150 mm, respectively.

amount of the mixture to the combustion chamber, incoming mass flow rate is controlled by the injection characteristics such as a total pressure p_0, a total temperature T_0, and an injection area ratio AR, defined as the net area of injector throats by the net area of injection wall. The injection system is modeled with three different injection conditions, depending on the left-wall pressure as follows. The first condition is illustrated in Fig. 2a where the detonation wave is located just in the front of an injector so that the wall pressure is greater than the injection total pressure. In this case, injection flow properties are obtained by assuming that the flow in the injection system is isentropic as

$$p = p_w, \qquad T = T_0\left(\frac{p}{p_0}\right)^{\frac{\gamma-1}{\gamma}} \quad \text{and} \quad u = 0 \tag{6}$$

where p_w is the left-wall pressure. In the second condition shown in Fig. 2b, the wall pressure is less than the injection total pressure, but greater than the critical pressure obtained at a choking condition. The injection flow properties are, thus, obtained by

$$p = p_w$$

$$T = T_0\left(\frac{p}{p_0}\right)^{\frac{\gamma-1}{\gamma}} \quad \text{and} \quad u = \sqrt{\frac{2\gamma}{\gamma-1}RT_0\left[1-\left(\frac{p}{p_0}\right)^{\frac{\gamma-1}{\gamma}}\right]} \tag{7}$$

The injection flow properties for the last condition are computed as

$$p = p_{\text{cr}}, \qquad T = T_0\left(\frac{p}{p_0}\right)^{\frac{\gamma-1}{\gamma}} \quad \text{and} \quad u = \sqrt{\frac{2\gamma}{\gamma+1}RT_0} \tag{8}$$

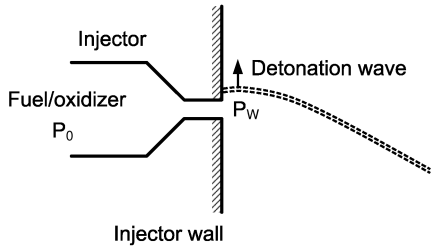

a) No injection: $p_w \geq p_0$

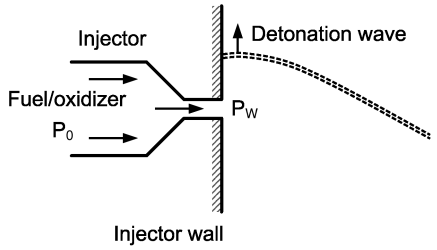

b) Subsonic injection: $p_0 > p_w > p_{cr}$

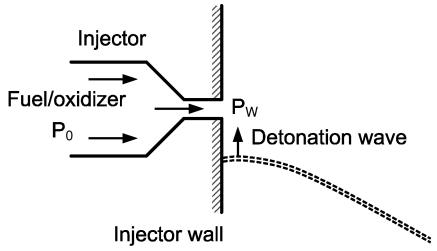

c) Sonic injection: $p_w \leq p_{cr}$

Fig. 2 Injection conditions based on the left-wall pressure in the front of an injector.

where the critical pressure p_{cr} is defined by

$$p_{\text{cr}} = p_0\left(\frac{2}{\gamma+1}\right)^{\frac{\gamma}{\gamma-1}} \tag{9}$$

In this case where the detonation wave propagates far from or before the injector as shown in Fig. 2c, the wall pressure is less than the critical pressure.

III. Verification of Code and Chemical Kinetics

A. Characterization of Thermochemical Parameters

Because a wide range of initial pressure and temperature is used in this study, the one-step model of hydrogen and air kinetics is validated accordingly. One-dimensional detonation in a 0.5 m long tube is compared with theoretical values obtained from CEA [23]. The detonation tube is modeled with the grid size of 0.1 mm. The detonation is directly initialized on the left-end wall of the tube filled with the hydrogen-air mixture at $p = 1$ to 4 atm, $T = 300$ to 500 K and $V = 0$ m/s. The thermodynamic and chemical parameters are adopted from Mall et al. [24] as

$$\gamma = 1.29, \qquad R = 368.9 \text{ J/kg} \cdot \text{K}$$
$$K = 7.5 \times 10^9 \text{ s}^{-1} \quad \text{and} \quad E_a = 4.794 \times 10^6 \text{ J/kg} \tag{10}$$

The total chemical energy release q is slightly modified from 2.8×10^6 J/kg for $T = 300$ K to 2.6×10^6 J/kg for $T = 500$ K, depending on the initial temperature. The values of q are used to obtain a maximum error less than 8% in both Chapman–Jouguet (CJ) pressure and temperature. With these parameters, the computed CJ pressure and temperature are always higher and lower than the theoretical values, respectively. Shown in Figs. 3a–3c, the computed detonation velocities at all the ranges of initial conditions are close to

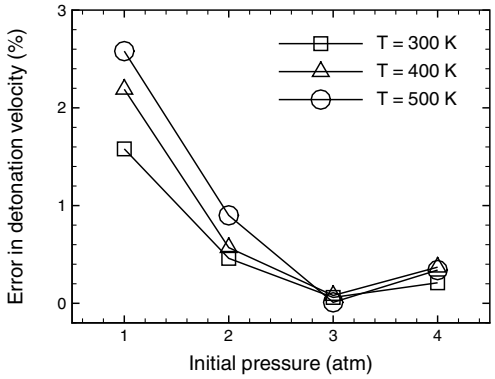

a) Error in Detonation velocity

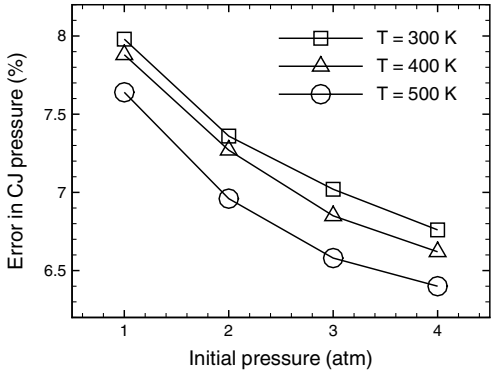

b) Error in CJ pressure

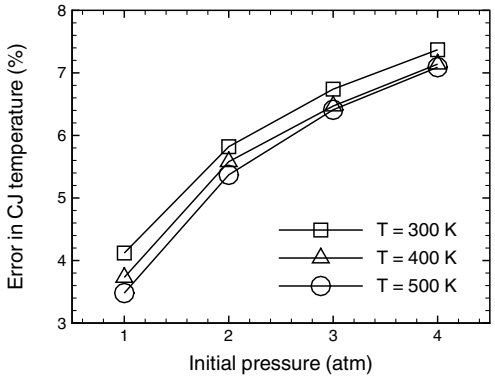

c) Error in CJ temperature

Fig. 3 Comparison of detonation properties in a one-dimensional tube with theoretical values.

the theoretical values, whereas the computed CJ pressure and temperature differ by 3 to 8%. These trends of errors in the one-step model were also presented by Ma et al. [24].

One of those calculations is given in detail. The one-dimensional detonation velocity, pressure and temperature at the initial conditions of $p = 2$ atm and $T = 400$ K is compared with theoretical values computed by CEA [23]. These initial conditions are chosen as the average values of the mixture just in front of the detonation wave in RDE with baseline conditions. The theoretical CJ detonation velocity, pressure and temperature corresponding to these initial conditions are 1979.1 m/s, 23.64 atm and 3028.9 K, respectively. The CJ detonation velocity, pressure and temperature of the one-step hydrogen and air model are computed as 1990.5 m/s, 25.49 atm and 2868.9 K, respectively.

The stability of detonation depends on the ratio of specific heats, chemical heat release and activation energy. The detonation is generally more stable if chemical heat release or activation energy decreases at a given specific heat ratio [25]. With the parameters given in Eq. (10), the equivalent dimensionless values of the chemical heat release [22] are computed as 25.3, 18.3, and 14.1 for $T = 300$–500 K, and the dimensionless activation energies are 43.3, 32.5, and 26.0, respectively. Thus, the detonation with these chemical parameters becomes more stable as the initial temperature increases. Moreover, the regime of detonation stability can be classified in terms of reduced activation energy $\Theta = E_a/RT_{\mathrm{VN}}$ and CJ Mach number where T_{VN} is the temperature at a von Neumann pressure peak [26,27]. The reduced activation energies are ranged between about 4 to 4.5 with the parameters given in Eq. (10), which correspond to the category of weakly unstable detonations.

B. Study of Grid Dependence

It is well known in numerical detonation simulation that a minimum of 20 grid points is required in a half-reaction zone to accurately capture detailed detonation structure or detonation instability. Shepherd [28] experimentally showed that the reaction zone of detonation has a significant spatial gradient on the order of $1 \sim 10$ μm. Wescott et al. [29] used 20 grid points in a half-reaction zone to capture a detonation wave turning a corner. Choi et al. [27] reported that an accurate simulation of detonation cell structures requires at least five grid points in the heat-release zone of steady ZND detonation. In an engine performance study, however, it is not practical, nor is it necessary to use such finer grid owing to a significant increase in computational time and resource as argued by Ma et al. [24], Morris [30], and Harris et al. [31], who used the grid size of 0.2 mm, 0.1 mm, and 0.6 mm, respectively. They found that the chosen grid can capture the accurate CJ properties of stable detonation without capturing detailed detonation front structure.

To confirm grid dependence on the CJ properties of stable detonation, the comparison of one-dimensional detonation velocity, pressure and temperature with four different grid sizes is performed and is shown in Table 1. Based on the observation from the table, the grid of $\Delta x = 0.1$ mm is chosen for the study of propulsive performance with baseline injection conditions, whereas the grid of $\Delta x = 0.2$ mm is used for the parametric study of propulsive performance.

In addition to the grid dependence on detonation CJ properties, the grid dependence on propulsive parameters is discussed in the following. The propulsive performance of one-waved RDE in a 0.1×0.2 m chamber with a grid size of 0.125 mm is first evaluated up to $t = 3$ ms. The injection conditions are used as $p_0 = 5$ atm, $T_0 = 400$ K and AR $= 0.15$. In the evaluation of engine performance with a finer grid such as $\Delta x = 0.0625$ or 0.03125 mm, a RDE chamber is initialized with the results of the coarser grid case at $t = 3$ or 3.2 ms, respectively. In the finest case, 12.5 grid points are used in the half-reaction zone. Even though the finest grid resolution may not be enough to resolve the detailed structure of reaction zone in the detonation, some main features of detonation wave in the RDE are approximately captured, as shown in Fig. 4 where the features include incident shocks, Mach stems, triple points, transverse waves and reaction zones (not shown in the figure).

The temporal evolution of fuel-based specific impulse of the one-waved RDE with three different grid sizes is presented in Fig. 5 after the flowfield is stabilized. The difference in the thrust between the coarsest and finest grids is only 0.487% as given in Table 2, where F and $I_{\mathrm{sp},f}$ denote the weighted-average thrust and fuel-based specific impulse, respectively, with respect to time. The difference in the fuel-based specific impulse is 3.979% between the coarsest and finest

Table 1 Comparison of one-dimensional detonation properties at $p = 2$ atm and $T = 400$ K with different grid resolutions

Δx, mm	U_D, m/s	p_{CJ}, atm	T_{CJ}, K
0.4	1986.3	25.37	2866.3
0.2	1990.5	25.48	2869.5
0.1	1990.5	25.49	2868.9
0.05	1994.7	25.47	2868.4

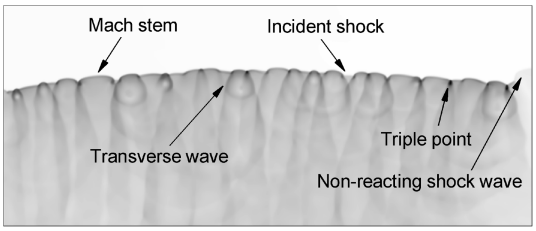

Fig. 4 Detonation wave captured with the grid size of 0.03125 mm.

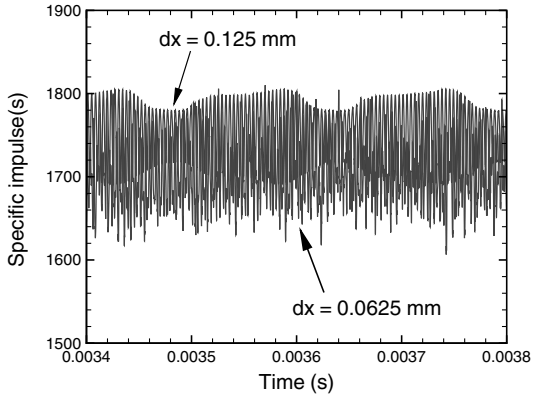

a) Comparison of fuel-based specific impulse of RDE between Δx = 0.125 and 0.0625 mm

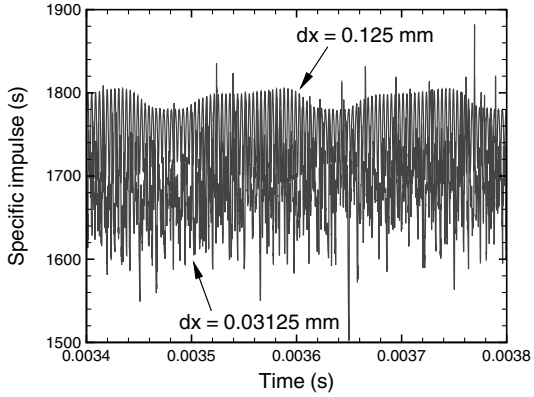

b) Comparison of fuel-based specific impulse of RDE between Δx = 0.125 and 0.03125 mm

Fig. 5 Comparison of fuel-based specific impulse of RDE with three different grid resolutions.

grids. Note that the fuel-based specific impulse is a function of flow properties at the chamber inlet and outlet. As shown in Fig. 5 and Table 2, the difference in the propulsive parameters of the RDE among three grid resolutions is negligible. Therefore, without capturing the detonation instability, it is possible to evaluate accurately the propulsive performance of RDE. Because this work is intended to analyze the propulsive performance of the engine, and not to analyze the detonation instability or detonation front structure, the chosen grid size of 0.1 mm is deemed adequate to achieve both numerical efficiency and accuracy.

Table 2 Comparison of propulsive parameters with three different grid resolutions

Δx, mm	0.125	0.0625	0.03125
F, kN/m	15.816	15.745	15.739
ΔF, %	-	0.449	0.487
$I_{sp,f}$, s	1753.87	1702.37	1684.09
$\Delta I_{sp,f}$, %	-	2.936	3.979

IV. Results and Discussion

Detonation waves are modeled in a 0.177 m long and 0.471 m high RDE chamber initially filled with a hydrogen and air mixture at the pressure of 1 atm and the temperature of 400 K. The detonation waves obtained from the one-dimensional simulation are mapped onto the left wall so that they propagate into the upper boundary of the chamber. For this study, baseline conditions are set as the two-waved RDE with injection conditions of 10 atm in a total pressure, 500 K in a total temperature and 0.2 in an injection area ratio. These total pressure and temperature are assumed as those just before entering a combustion chamber. Thus, the effects of an inlet on the pressure such as a total pressure recovery and a pressure loss across manifold [24] are ignored in this study. The flight condition is assumed as the Mach number of 1.5 at the altitude of 5.5 km for the thrust evaluation.

A. Overall Features of Continuously Rotating Detonation with Baseline Conditions

Two detonation waves successively propagating in the azimuthal direction of the RDE chamber are presented in Fig. 6 where the detonations are moving to the upper boundary. Most features observed in the experiment [8] are depicted in the figure, including combustible mixture layers, detonation waves followed by combustion product expansions and contact surfaces emanating from the right end of a detonation wave. The fresh mixture is continuously injected from the left wall of the chamber, resulting in the formation of a triangular layer and it flows into the axial direction of the chamber. The mixture properties in the layer are nonuniform due to the influence of the combustion product expansion of a prior detonation wave. The pressure and temperature of the mixture immediately in the front of the detonation wave near the left wall are approximately 1.97 atm and 474 K, respectively. Across the axial direction of the chamber, they gradually decrease to lowest values at the right end of the mixture layer as 1.18 atm and 357 K. The axial velocity of the mixture is ranged from 280 m/s around the left wall to 480 m/s at the right end, which corresponds to the Mach number of 0.65 and 1.17, respectively. In Fig. 6, the triangular layer is roughly 29 mm long and 202 mm high, including the region of the small amount of the mixture. The layer thickness is directly proportional to

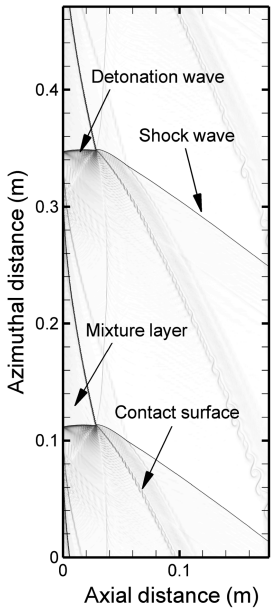

Fig. 6 Density gradient of detonation waves in two-waved RDE with baseline conditions at $t = 5 \times 10^{-3}$ s.

the duration between the successive detonation waves and it is one of critical factors in the operation of the RDE [8].

One of the typical features of detonation wave in the RDE is that the wave is inclined backward on the left wall due to mixture injections and its wave strength varies across the axial direction. The ratios of the pressures and temperatures ahead of and behind the detonation wave are computed as $p_1/p_2 = 15.04$ and $T_1/T_2 = 6.40$ at $x = 0.005$ m. These ratios gradually increases to $p_1/p_2 = 17.26$ and $T_1/T_2 = 8.26$ at $x = 0.025$ m. The temporal evolution of the pressure at $x = 0.005$ m on the upper boundary of the chamber is presented in Fig. 7 to demonstrate the stability in the engine operation. After eight cycles, the flowfield is stabilized and the peak pressure reaches roughly 29 atm. Two contact discontinuities are emanated from the right end of the detonation wave, one is moving to the chamber exit and the other is connected to the right end of the next detonation wave. As the result of the combustion product expansion, a nonreacting shock wave is generated from the right end of the detonation and propagates at a supersonic speed into the chamber exit. In Fig. 6, the shock wave is steeply inclined backward by about 36°. This angle depends on the detonation velocity, i.e., the type of a fuel-oxidizer mixture and its conditions. The strength of this shock wave gradually decreases across the axial direction of the chamber such that $p = 4.35$ atm at $x = 0.1$ m and $p = 3.66$ atm at $x = 0.15$ m after stabilized. The hot expansion wave is also interacting with the fresh mixture, resulting in the mixture burning on a contact surface.

The detonation properties on the inlet and outlet of the RDE chamber are presented in Fig. 8 where the detonation waves propagate from the left to the right. The figures show that the inlet pressure and temperature immediately in the front of the detonation wave are approximately 0.93 atm and 398 K. At these conditions with the zero velocity, the theoretical CJ detonation pressure, temperature and velocity are computed as 10.9 atm, 2969 K, and 1962 m/s, respectively. As also shown in Fig. 8, the pressure behind the detonation wave gradually decreases to roughly 8 atm at the starting point of the mixture layer. After this point, the pressure oscillation occurs due to the interaction between the expansion wave and the left wall. On the other hand, the temperature steeply decreases until the expansion wave reaches the fresh mixture layer. In Fig. 8c, the velocity immediately behind the detonation wave on the inlet is negative, which means that a reverse flow occurs in the front of an injector. At the chamber exit, the weighted-average pressure, temperature, and velocity are 2.02 atm, 1824.3 K, and 1004.7 m/s, respectively. This velocity corresponds to the Mach number of 1.08. The detonation velocity computed at the inlet is 1945 m/s after the flowfield is stabilized so that the frequency of the two-waved RDE is obtained as [8]

$$f = \frac{N_w U_D}{\pi d} = 8.26 \text{ kHz} \tag{11}$$

where N_w is the number of detonation waves resided in the chamber, U_D is the detonation velocity and d is the outer diameter of the chamber. Note that a variable in the abscissa is used as the weighting variable throughout this work.

B. Propulsive Performance of RDE with Baseline Conditions

The propulsive performance of the two-waved RDE shown in Fig. 6 is evaluated in terms of mass flow rate, thrust, specific impulse and total pressure loss. The thrust due to a change in momentum at the chamber exit is obtained by

$$F(t) = \int_{\text{exit}} [\rho u^2 + (p - p_\infty)] \, \mathrm{d}l - \dot{m}_a u_\infty \tag{12}$$

where $F(t)$ is integrated along the azimuthal direction of the chamber, p_∞ is the ambient air pressure and $\dot{m}_a$ is the mass flow rate of air delivered to an inlet or a combustion chamber in a unit of kg/s · m. The total impulse is defined as

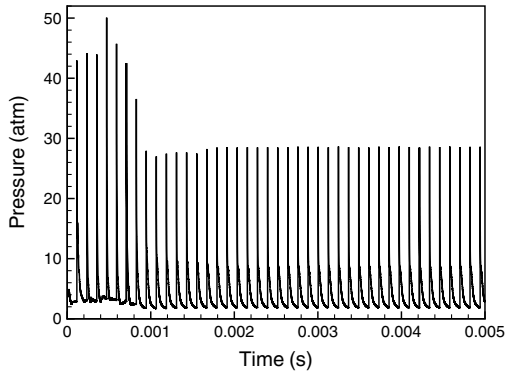

Fig. 7 Temporal variation of the pressure at $x = 0.005$ m on the upper boundary of the combustion chamber up to 5×10^{-3} s.

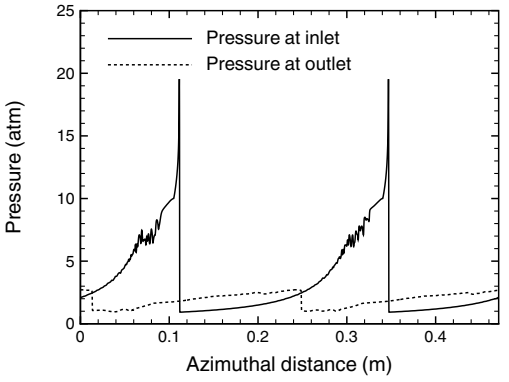

a) Pressure profile

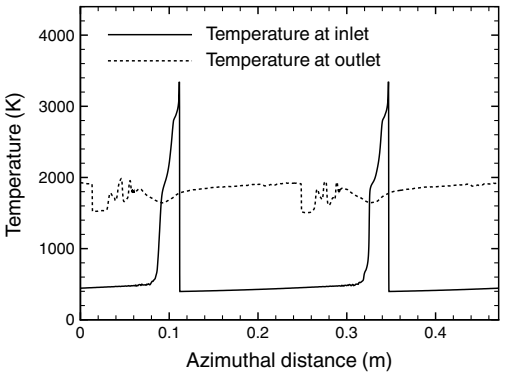

b) Temperature profile

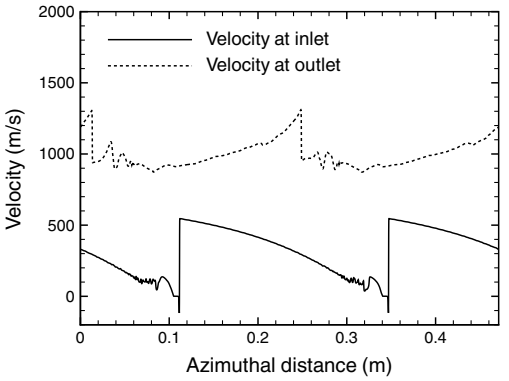

c) Velocity profile

Fig. 8 Detonation properties on the inlet and outlet of two-waved RDE with baseline conditions at $t = 5 \times 10^{-3}$ s.

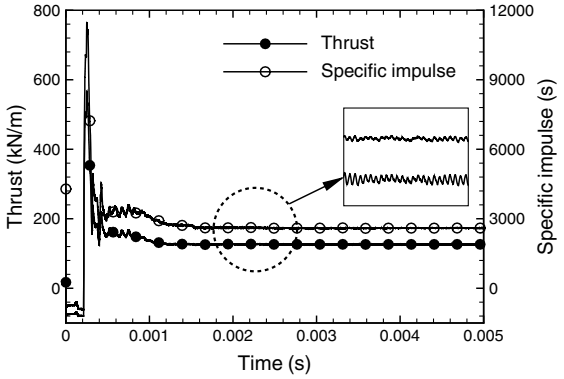

a) Temporal evolution of thrust and fuel-based specific impulse per unit depth

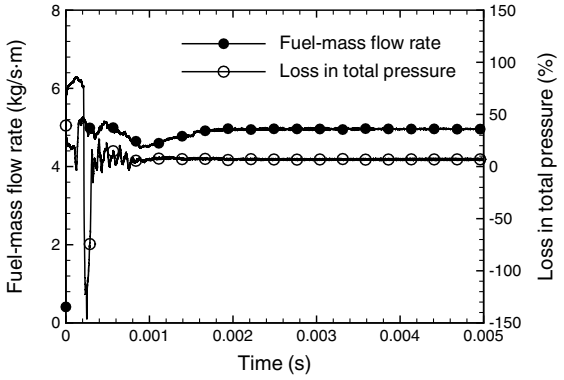

b) Temporal evolution of fuel-mass flow rate per unit depth and a total pressure loss

Fig. 9 Propulsive performance of two-waved RDE with baseline conditions.

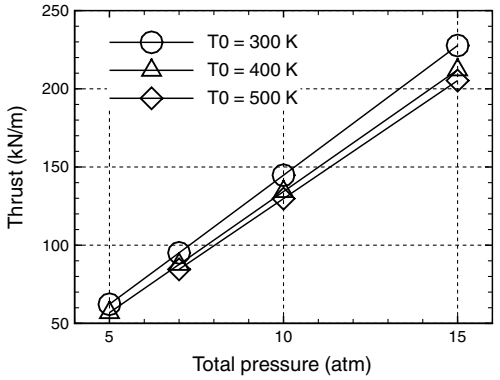

a) Weighted-average thrust versus injection total pressure

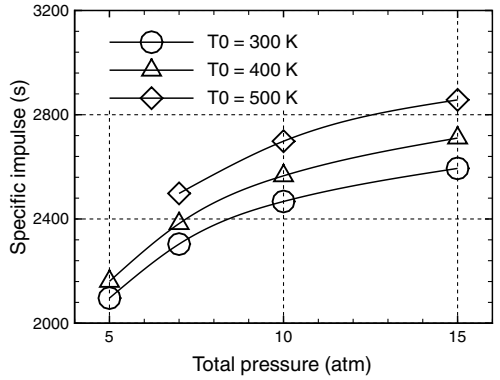

b) Weighted-average fuel-based specific impulse versus injection total pressure

Fig. 10 Propulsive performance of two-waved RDE with injection total temperatures at AR = 0.2.

$$I(t) = \int F(t)\,\mathrm{d}t \tag{13}$$

This total impulse is evaluated in the last section to compare the propulsive performance between the RDE and PDE. The specific impulse is a measure of engine efficiency and is defined as the thrust per unit propellant weight. In this study, the specific impulse of the RDE is fuel-based and equated with

$$I_{\mathrm{sp},f}(t) = \frac{F(t)}{g_0 \dot{m}_f(t)} \tag{14}$$

where g_0 is the gravity acceleration. The fuel-mass flow rate on the injection wall is defined as

$$\dot{m}_f(t) = \int \rho_f u\,\mathrm{d}l \tag{15}$$

where ρ_f is the fuel density. Note that these propulsive parameters are time-dependent quantities.

The temporal evolution of the thrust and fuel-based specific impulse per unit depth of the two-waved RDE is plotted in Fig. 9a up to 5×10^{-3} s. After large variations at the early time, the thrust and fuel-based specific impulse converge to the approximately constant values of 126.3 ± 0.2 kN/m and 2597 ± 6 s, respectively. They have repetitively small variations with time due to the influence of the combustion product expansion as shown in the figure. The thrust peak at the very beginning is due to the interaction between detonation and shock waves in the engine initiation. The thrust converges to the constant value after about $t = 1.2$ ms. On the other hand, the fuel-mass flow rate given in Fig. 9b also approaches to the constant value of 4.959 ± 0.004 kg/s · m. Unlike the thrust, the average fuel-mass flow rate at the beginning is lower than its overall average and it takes longer to be stabilized. Another important parameter that indicates the engine performance is a total pressure loss due to shock waves resided in the combustion chamber. As shown in Fig. 9b, the total pressure loss converges to about $6.88 \pm 0.07\%$ after stabilized. The weighted-average total pressures at the inlet and outlet of the chamber are 4.205 and 3.914 atm in the figure, respectively. Hence, the weighted-average total pressure loss at the chamber exit is evaluated as 6.92%.

C. Effect of Injection Conditions on Propulsive Performance

The influence of injection conditions such as the total pressure, total temperature and injection area ratio on the propulsive performance of the two-waved RDE is investigated in the 0.177 m long and 0.471 m high chamber. The injection conditions are ranged as the total pressure of 5–15 atm, the total temperature of 300–500 K and the injection area ratio of 0.1–0.4. The propulsive parameters formulated in the previous section are also evaluated along the azimuthal direction up to 5×10^{-3} s in this section.

The weighted-average thrust and fuel-based specific impulse per unit depth with respect to the various injection total pressures and temperatures are estimated in Fig. 10. The thrust was not evaluated for the case of $p_0 = 5$ atm and $T_0 = 500$ K since the mixture layer was not properly formed due to the low mass flow rate. The thrust linearly increases with increasing the injection total pressure, but decreases with increasing the injection total temperature. The RDE with those injection conditions also produces the roughly constant thrust just like that plotted in Fig. 9a. As mentioned in Sec. IV.B, the RDE has slight thrust variations with time after stabilized. This is caused by the flowfield disturbance due to the combustion product expansion of the prior detonation wave. This disturbance increases as the injection total temperature increases, resulting in the relatively higher variations of the thrust. The fuel-based specific impulse also increases with increasing the injection total pressure, but its rate of increase is less than that of the thrust due to the injected fuel-mass

flow rate that has the same trend. The behavior of the injection total temperature on the fuel-based specific impulse is different from that on the thrust as shown in Fig. 10b where the fuel-based specific impulse increases with the total temperature.

The evaluation of the thrust and fuel-based specific impulse per unit depth in terms of the injection area ratios at $T_0 = 500$ K is presented in Fig. 11. For the injection area ratio of 0.1, the RDE is operated only in the case of $p_0 = 15$ atm. In other conditions with AR = 0.1, the operation of the RDE cannot occur since the triangle layer of the mixture is not properly formed. The thrust and fuel-based specific impulse increase by increasing the injection area ratio as shown in Fig. 11. Thus, the propulsive parameters are strongly dependent on the injection area ratio. As the injection area ratio increases, the mixture pressure and axial velocity immediately in the front of the detonations increases linearly, but the mixture temperature remains constant. These behaviors of the mixture layer and propulsive performance of the RDE on the injection area ratio are also presented in Table 3 where $\dot{m}_M$ and Δp_0 denote the mixture-mass flow rate and the loss in the total pressure, respectively. Note that the mixture properties in the table are ranged from the left wall to the right end of the mixture layer.

D. Effect of Other Parameters on Propulsive Performance

The propulsive parameters of the RDE that has three different numbers of detonation waves ($N_w = 1$, 2, and 4) and three different axial chamber lengths ($L_x = 0.1$, 0.177, and 0.3 m) are evaluated to investigate their effects on the engine performance. Figures 12a and 12b depict the detonation waves continuously propagating in the one- and four-waved RDE, respectively. The typical features of the RDE are also captured in the figures and the overall structure is quite similar to the two-waved RDE except the mixture layer thickness, which is obtained as approximately 55.6 mm in Fig. 12a and 14.7 mm in Fig. 12b. These are about two and one-half times thicker than that of the two-waved RDE. Note that the mixture layer thickness directly depends on the duration between successive detonations. Moreover, the overall structure of the 0.1 and 0.3 m long RDE is also identical to that of the baseline RDE.

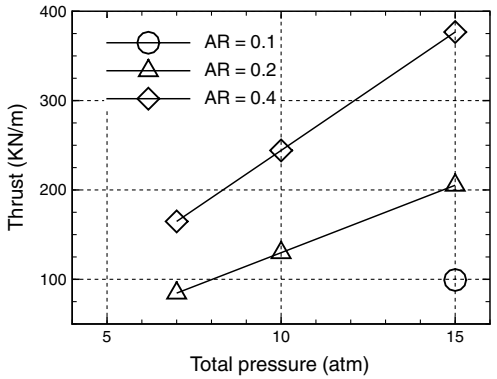

a) Weighted-average thrust versus injection total pressure

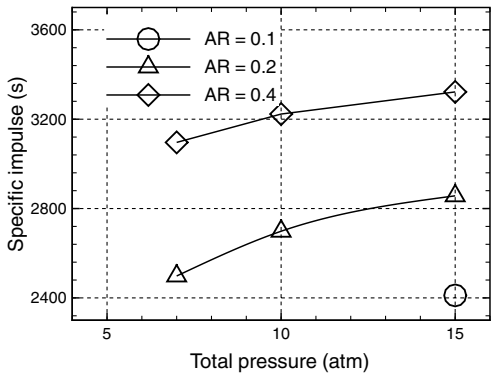

b) Weighted-average fuel-based specific impulse versus injection total pressure

Fig. 11 Propulsive performance of two-waved RDE with injection area ratios at $T_0 = 500$ K.

1. *Number of Detonation Waves*

The influence of the number of detonation waves on the engine performance is given in Table 4. The table presents the propulsive performance of the one-, two-, and four-waved RDE in terms of the weighted-average mixture-mass flow rate, fuel-mass flow rate, thrust, fuel-based specific impulse and total pressure loss. By increasing the number of the detonation waves, the RDE delivers almost the same performance. For example, the difference between the thrusts and specific impulses of the one- and four-waved RDE is 0.898 and 1.856%, respectively. However, the loss in the total pressure increases when the number of shock waves increases. From the table, the difference between the total pressure losses of the one- and four-waved RDE is 10.9%. As shown in Fig. 13a, the thrusts generated by the one-, two-, and four-waved RDE converge to the approximately same constant value. Because the number of the detonation waves rotating in the RDE depends on the chamber diameter after stabilized, a further increase in the number of waves results in the failure of operating the RDE.

2. *Axial Chamber Lengths*

The evaluation of the propulsive parameters of the two-waved RDE with three different chamber lengths is also performed in this section and presented in Table 5. The influence of the axial chamber lengths on the engine performance is insignificant as shown in the table as well as Fig. 13b where all the thrusts converge to the roughly same constant value. However, as expected, the RDE takes longer to reach the stable operation as the chamber length increases. From the table, the difference in the thrust and specific impulses between the 0.1 and 0.3 m long chambers is computed as 3.073 and 4.675%, respectively, while the difference between the total pressure losses is about 10.6%. Davidenko et al. [17] studied the effect of the chamber length on the flowfield structure with much shorter chambers (less than 0.1 m). He concluded that the RDE can be operated in the chamber of which the length is a few times longer than the mixture layer thickness. Bykovskii et al. [8] also found experimentally that the minimum chamber length is approximately 2 times as long as a critical mixture layer thickness.

Table 3 Influence of injection area ratio on mixture layer and propulsive performance of two-waved RDE with $p_0 = 15$ atm and $T_0 = 500$ K

AR	0.1	0.2	0.4
p_M, atm	1.51–1.17	2.88–2.14	5.38–4.01
T_M, K	476–415	474–408	471–417
u_M, m/s	268–365	280–403	303–420
$\dot{m}_M$, kg/s · m	141.25	248.24	393.64
$\dot{m}_f$, kg/s · m	4.03	7.08	11.22
F, kN/m	99.26	205.27	376.72
$I_{sp,f}$, s	2411.2	2857.0	3322.1
Δp_0, %	5.17	7.23	8.80

Table 4 Influence of the number of detonation waves on engine performance with baseline injection conditions and $L_x = 0.177$ m

N_w	1	2	4
$\dot{m}_M$, kg/s · m	173.52	173.12	171.90
$\dot{m}_f$, kg/s · m	4.95	4.94	4.90
F, kN/m	126.99	127.67	128.13
$I_{sp,f}$, s	2618.7	2638.9	2667.3
Δp_0, %	6.70	6.92	7.43

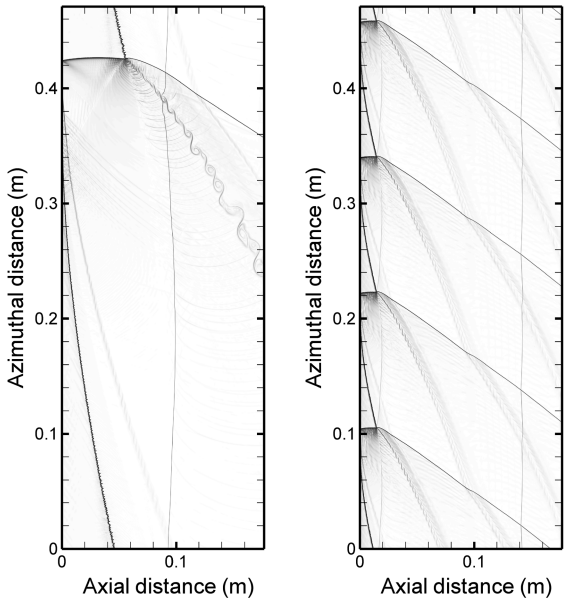

a) One-waved RDE **b) Four-waved RDE**

Fig. 12 Density gradient of detonation waves in one- and four-waved RDE with baseline injection conditions at $t = 5 \times 10^{-3}$ s.

E. Comparison of Propulsive Performance Between RDE and PDE

The thrust and total impulse per unit area of the two-waved RDE with the baseline injection conditions are compared with those of the one-dimensional PDE that has a 0.5 m long tube with no nozzle. The detonation in the PDE is initialized on the left closed-end and propagates to the right open-end. The typical operating cycle of the PDE is based on the valve open and closed period [24], which has four basic modes: purging and filling, initiating, propagating, and exhausting (blowdown) processes. For this study, the cycle period is chosen as $t_{\text{cycle}} = 1.9$ ms, which corresponds to the operating frequency of 526.3 Hz. This frequency of the PDE is so high for practical use. Thus, it was adopted for a comparison only. The operating cycle consists of the valve closed period $t_{\text{closed}} = 1.35$ ms, the purging period $t_{\text{purging}} = 0.05$ ms and the filling period $t_{\text{filling}} = 0.5$ ms. In the purging and filling modes, the pressure and temperature are set to 1.58 atm and 416 K, respectively, since these are the averaged values of the mixture immediately in the front of the detonation waves in the RDE shown in Fig. 6. The PDE operation was stabilized after three cycles and the peak thrust reaches 9720 kN/m^2.

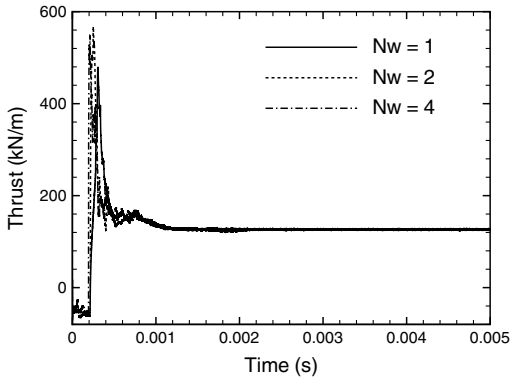

a) Comparison of thrust with different number of detonation waves at $L_x = 0.177$ m

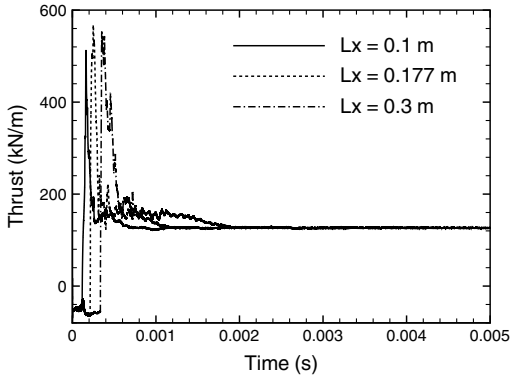

b) Comparison of thrust with different axial chamber lengths at $N_w = 2$

Fig. 13 Influence of the number of detonation waves and axial chamber lengths on thrust with baseline injection conditions.

Table 5 Influence of axial chamber lengths on engine performance with baseline injection conditions and $N_w = 2$

L_x, m	0.1	0.177	0.3
$\dot{m}_M$, kg/s · m	173.80	173.12	171.27
$\dot{m}_f$, kg/s · m	4.96	4.94	4.88
F, kN/m	126.57	127.67	130.46
$I_{sp,f}$, s	2605.2	2638.9	2727.0
Δp_0, %	6.79	6.92	7.51

Because of the continuous operation of the RDE, it has several advantages in producing thrust, compared with the PDE. As shown in Fig. 14a where the comparison of the thrust per unit area between the RDE and PDE is presented, the RDE produces the constant thrust after stabilized. However, the PDE generates the repetitive and intermittent thrust, which causes unwanted higher vibration and noise of the engine. In the figure, the period of the blowdown process takes roughly 58% of a cycle and the most thrust is produced in the early period of this process. The PDE produces a higher thrust only at the short period when the detonation is leaving the tube. From Fig. 14a, the weighted-average thrust produced by the RDE and PDE is obtained as 268.9 and 202.3 kN/m^2, respectively. Another advantage is that the RDE is operated at a very high frequency by a continuous fuel-oxidizer supply to the combustion chamber. The frequency of the RDE modeled in this study is obtained to be 8.26 kHz, which indicates that the thrust in Fig. 14a results from the 41.3 rotations of each detonation wave in 0.01 s. On the other hand, because of purging and filling processes in the PDE operation, it is difficult to obtain high operating frequency, resulting in lower thrust. The period of these processes takes about 29% of the cycle, but the PDE produces only 8.34% of the thrust during the cycle. The temporal evolution of the total impulse per unit area of the RDE and PDE is presented in Fig. 14b. The total impulse of the RDE linearly increases with time, but the PDE shows the discontinuous behavior in the total impulse, which is caused by a sudden increase in the thrust. The RDE produces the total impulse of 2708.1 N · s/m^2 at $t = 0.01$ s. This is 38.7% higher than that produced by the PDE.

F. Comparison of Propulsive Performance with Other Studies on RDE and PDE

There have been few other attempts to experimentally and numerically analyze the propulsive performance of RDE in which comparison can be made with the current work although reference data published in the literature are very limited. One of them is Daniau et al. [10], who experimentally measured the thrust of 2750 N in a small rocket chamber. He used a kerosene-oxygen mixture in a 50 mm diameter and 100 mm long chamber with the mixture mean pressure of 0.5 MPa to 0.7 MPa, which is much higher than the baseline injection conditions used in this study. Another comparison can be made with that of Hishida et al. [18], who numerically studied two-dimensional RDE with a 70% argon-diluted hydrogen and oxygen mixture in a 0.2 m long square chamber. He obtained the thrust and fuel-based specific impulse of 60 kN/m and 4700 s,

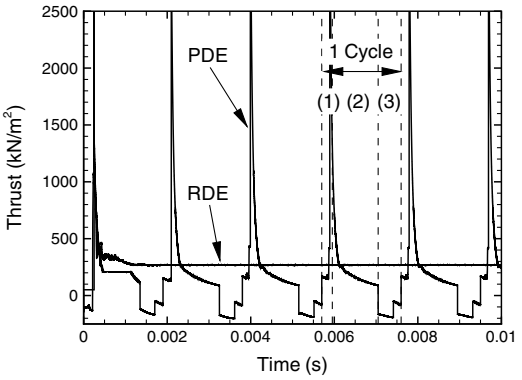

a) Temporal evolution of thrust per unit area

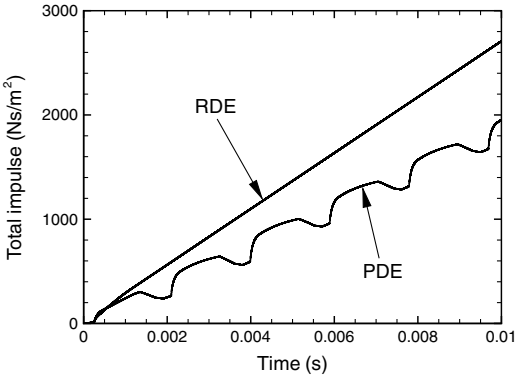

b) Temporal evolution of total impulse per unit area

Fig. 14 Comparison of propulsive performance between RDE and PDE: 1) propagating process: 0.253 ms, 2) blowdown process: 1.097 ms, and 3) purging and filling process: 0.55 ms.

respectively, after the flowfield was stabilized. The thrust and fuel-based specific impulse of the RDE modeled in this study were 1182.6 N and 2638.89 s with the baseline injection conditions, and 1916.7 N and 2957.0 s with the injection conditions of $p_0 = 15$ atm, $T_0 = 500$ K, and AR $= 0.2$.

On the other hand, there exists a large volume of study on the propulsive performance of single- or multiple-tube PDE with a hydrogen-air mixture in the literature. Ma et al. [24] investigated the propulsive performance of PDE in a 0.16 m diameter and 0.6 m long chamber without a nozzle. He obtained the fuel-based specific impulse of 2355 s with the flight conditions of $M_\infty = 2.1$ at the altitude of 9.3 km. If the same flight conditions are used, the RDE produces the thrust and fuel-based specific impulse of 1196.4 N and 2667.3 s, respectively, with the baseline injection conditions.

V. Conclusions

The propulsive performance of a continuously rotating detonation engine with an annular chamber was numerically investigated. The effect of various engine design parameters including injection conditions, axial chamber length, and the number of detonation waves on the engine performance were studied systematically. The rotating detonation engine fueled with a hydrogen–air mixture was modeled in a two-dimensional chamber simplified from an actual chamber used in experiments. A computational code was based on two-dimensional Euler equations associated with the one-step Arrhenius kinetics of the hydrogen-air mixture.

All typical features, that are observed in experiments, of the continuously rotating detonation engine were captured and analyzed in this study. The features include the triangular layer of an injected mixture, a curved detonation wave followed by a combustion product expansion, a contact surface emanating from the right end of a detonation wave, and a nonreacting shock wave propagating into the chamber exit at a supersonic speed. It was shown that the rotating detonation engine was operated at a very high frequency, running at 8.26 kHz and produces approximately a constant thrust. Moreover, it was demonstrated that the rotating detonation engine produces a total impulse higher than that of a single-tube pulse detonation engine. It was found that the propulsive performance of the rotating detonation engine is strongly dependent on injection flow conditions, which are engine design parameters to determine the mass flow rate of an injected mixture. The engine performance increases with increasing injection total pressure and area ratio. However, the effect of the axial chamber length and the number of detonation waves, which are geometric design parameters, is insignificant on the engine performance. The operation of the rotating detonation engine will be failed if the mass flow rate is lower or higher than its range obtained at specific mixture conditions. Thus, the proper formation of a triangular mixture layer is a key factor to achieve a stable engine operation.

Acknowledgments

This work was supported by the Agency for Science, Technology and Research (A*STAR), Singapore under Grant IHPC06-201802. The first author would like to thank D.M. Davidenko for useful discussions on injection boundary conditions, B.C. Khoo for discussions on the detonation physics, and J. Powers for helpful suggestions to improve this manuscript.

References

[1] Roy, G. D., Frolov, S. M., Borisov, A. A., and Netzer, D. W., "Pulse Detonation Propulsion: Challenges, Current Status and Future Perspective," *Progress in Energy and Combustion Science*, Vol. 30, No. 6, 2004, pp. 545–672. doi:10.1016/j.pecs.2004.05.001

[2] Hinkey, J. B., Williams, J. T., Henderson, S. E., and Bussing, T. R. A., "Rotary-Valved, Multiple-Cycle, Pulse Detonation Engine Experimental Demonstration," AIAA Paper 1997-2746, 1997.

[3] Bussing, T. R. A., Lidstone, G., Christofferson, E., Kaemming, T., and Jones, G., "Pulse Detonation Propulsion Proof of Concept Test Article Development," AIAA Paper 2002-3633, 2002.

[4] Rasheed, A., Furman, A., and Dean, A. J., "Pressure Measurements and Attenuation in a Hybrid Multitube Pulse Detonation Turbine System," *Journal of Propulsion and Power*, Vol. 25, No. 1, 2009, pp. 148–161. doi:10.2514/1.31893

[5] Wilson, D. R., Lu, F. K., Kim, H., and Munipalli, R., "Analysis of a Pulsed Normal Detonation Wave Engine Concept," AIAA Paper 2001-1784, 2001.

[6] Kailasanath, K., "Research on Pulse Detonation Combustion Systems: A Status Report," AIAA Paper 2009-631, 2009.

[7] Voitsekhovskii, B. V., "Stationary Spin Detonation," *Soviet Journal of Applied Mechanics and Technical Physics*, Vol. 3, 1960, pp. 157–164.

[8] Bykovskii, F. A., Zhdan, S. A., and Vedernikov, E. F., "Continuous Spin Detonations," *Journal of Propulsion and Power*, Vol. 22, No. 6, 2006, pp. 1204–1216. doi:10.2514/1.17656

[9] Edwards, D. H., Parry, D. J., and Jones, A. T., "The Structure of the Wave Front in Spinning Detonation," *Journal of Fluid Mechanics*, Vol. 26, No. 2, 1966, pp. 321–336. doi:10.1017/S0022112066001265

[10] Daniau, E., Falempin, F., and Zhdan, S., "Pulsed and Rotating Detonation Propulsion Systems: First Step Toward Operational Engines," AIAA Paper 2005-3233, 2005.

[11] Falempin, F., and Daniau, E., "A Contribution to the Development of Actual Continuous Detonation Wave Engine," AIAA Paper 2008-2679, 2008.

[12] Bykovskii, F. A., Zhdan, S. A., and Vedernikov, E. F., "Continuous Spin Detonation of Hydrogen-Oxygen Mixtures. 1. Annular Cylindrical Combustors," *Combustion, Explosion, and Shock Waves*, Vol. 44, No. 2, 2008, pp. 150–162. doi:10.1007/s10573-008-0021-1

[13] Nicholls, J. A., Cullen, R. E., and Raglano, K. W., "Feasibility Studies of a Rotating Detonation Wave Rocket Motor," *Journal of Spacecraft and Rockets*, Vol. 3, No. 6, 1966, pp. 893–898. doi:10.2514/3.28557

[14] Wolanski, P., Kindracki, J., and Fujiwara, T., "An Experimental Study of Small Rotating Detonation Engine," *Pulsed and Continuous Detonations*, edited by G. D. Roy, S. M. Frolov, and J. Sinibali, Torus Press, Moscow, 2006, pp. 332–338.

[15] Wolanski, P., "Development of the Continuous Rotating Detonation Engines," *Progress in Pulsed and Continuous Det- onations*, edited by G. D. Roy, and S. M. Frolov, Torus Press, Moscow, 2009.
[16] Zhdan, S. A., Bykovskii, F. A., and Vedernikov, E. F., "Mathematical Modeling of a Rotating Detonation Wave in a Hydrogen-Oxygen Mixture," *Combustion, Explosion, and Shock Waves*, Vol. 43, No. 4, 2007, pp. 449–459.
doi:10.1007/s10573-007-0061-y
[17] Davidenko, D. M., Gökalp, I., and Kudryavtsev, A. N., "Numerical Study of the Continuous Detonation Wave Rocket Engine," AIAA Paper 2008-2680, 2008.
[18] Hishida, M., Fujiwara, T., and Wolanski, P., "Fundamentals of Rotating Detonation," *Shock Waves*, Vol. 19, No. 1, 2009, pp. 1–10.
doi:10.1007/s00193-008-0178-2
[19] Helzel, C., Leveque, R. J., and Warnecke, G., "A Modified Fractional Step Methods for the Accurate Appoximation of Detonation Waves," *SIAM Journal on Scientific Computing*, Vol. 22, No. 4, 2000, pp. 1489–1510.
doi:10.1137/S1064827599357814
[20] Tosatto, L., and Vigevano, L., "Numerical Solution of Under-Resolved Detonations," *Journal of Computational Physics*, Vol. 227, No. 4, 2008, pp. 2317–2343.
doi:10.1016/j.jcp.2007.10.011
[21] Berkenbosch, A. C., Kaasschieter, E. F., and Klein, R., "Detonation Capturing for Stiff Combustion Chemistry," *Combustion Theory and Modelling*, Vol. 2, No. 3, 1998, pp. 313–348.
doi:10.1088/1364-7830/2/3/006
[22] Williams, D. N., "Numerical Modelling of Multidimensional Detonation Structure," Ph.D. thesis, University of Calgary, Calgary, Alberta, 2002.
[23] Gordon, S., and McBride, B. J., "Computer Program for Calculation of Complex Chemical Equilibrium Compositions and Application I. Analysis," NASA Tech. Rept. RP-1311, 1976, http://www.grc.nasa.gov/WWW/CEAWeb [retrieved Oct. 2010].
[24] Ma, F., Choi, J. Y., and Yang, V., "Thrust Chamber Dynamics and Propulsive Performance of Single-Tube Pulse Detonation Engines," *Journal of Propulsion and Power*, Vol. 21, No. 3, 2005, pp. 512–526.
doi:10.2514/1.7393
[25] Lee, J. H. S., *The Detonation Phenomenon*, Cambridge Univ. Press, New York, 2008.
[26] Eckett, C. A., Quirk, J. J., and Shepherd, J. E., "The Role of Unsteadiness in Direct Initiation of Gaseous Detonations," *Journal of Fluid Mechanics*, Vol. 421, 2000, pp. 147–183.
doi:10.1017/S0022112000001555
[27] Choi, J. Y., Ma, F., and Yang, V., "Some Numerical Issues on Simulation of Detonation Cell Structures," *Combustion, Explosion, and Shock Waves*, Vol. 44, No. 5, 2008, pp. 560–578.
doi:10.1007/s10573-008-0086-x
[28] Shepherd, J. E., "Detonation in Gases," *Proceedings of the Combustion Institute*, Vol. 32, No. 1, 2009, pp. 83–98.
doi:10.1016/j.proci.2008.08.006
[29] Wescott, B. L., Stewart, D. S., and Bdzil, J. B., "On Self-Similarity of Detonation Diffraction," *Physics of Fluids*, Vol. 16, No. 2, 2004, pp. 373–384.
doi:10.1063/1.1633552
[30] Morris, C., "Numerical Modeling of Single-Pulse Gasdynamics and Performance of Pulse Detonation Rocket Engines," *Journal of Propulsion and Power*, Vol. 21, No. 3, 2005, pp. 527–538.
doi:10.2514/1.7875
[31] Harris, P. G., Stowe, R. A., Ripley, R. C., and Guzik, S. M., "Pulse Detonation Engine as a Ramjet Replacement," *Journal of Propulsion and Power*, Vol. 22, No. 2, 2006, pp. 462–473.
doi:10.2514/1.15414

J. Powers
Associate Editor